

RESEARCH

Open Access



Prognostic stratification based on HIF-1 α signaling for evaluating hypoxia status and immune landscape in hepatocellular carcinoma

Hongkai Zhuang^{1,2}, Zedan Zhang³, Bo Chen⁴, Chenwei Tang^{1,2}, Xinming Chen⁵, Wenliang Tan^{1,2}, Lei Yang^{1,2}, Zhiqin Xie^{1,2}, Xiaowu Ma^{1,2}, Qingbin Wang^{1,2}, Bingkun Wang^{1,2}, Changzhen Shang^{1,2*} and Yajin Chen^{1,2*}

*Correspondence:
shchzh2@mail.sysu.edu.cn;
chenyaj@mail.sysu.edu.cn

¹ Department of Hepatobiliary Surgery, Sun Yat-sen Memorial Hospital, Sun Yat-sen University, Guangzhou 510080, China

² Guangdong Provincial Key Laboratory of Malignant Tumor Epigenetics and Gene Regulation, Sun Yat-sen Memorial Hospital, Sun Yat-sen University, Guangzhou 510080, China

³ Department of Urology, Peking University First Hospital, Beijing 100034, China

⁴ Department of Breast Cancer, Guangdong Provincial People's Hospital (Guangdong Academy of Medical Sciences), Southern Medical University, Guangzhou 510080, Guangdong, China

⁵ Department of Hepatobiliary Surgery, Shenshan Medical Hospital, Sun Yat-sen Memorial Hospital, Sun Yat-sen University, Shanwei 516600, China

Abstract

Hepatocellular carcinoma (HCC) has a desmoplastic and hypoxic tumor microenvironment (TME), resulting in poor prognosis and treatment resistance. This study aimed to construct a novel prognostic classifier to investigate the degree of hypoxia and immune profiles in HCC. Patients with HCC from public databases were classified into three HIF-1 α clusters according to 16 reported HIF-1 α -related genes. Then, an HIF-1 α score system was constructed based on nine overlapping differentially expressed genes (ODEGs) among various HIF-1 α clusters. Then, an HIF-1 α score system was constructed based on nine overlapping differentially expressed genes (ODEGs) among various HIF-1 α cluster. Besides, oncologic pathways and immune infiltration profiles were also investigated among HCCs with different HIF-1 α scores. The reliable predictive abilities of the HIF-1 α score system for patients' survival were impressively suggested by the significant C-indexes and ROC analysis. All enrolled tumors were divided into high-, medium-, and low-HIF-1 α score groups. Compared with the other two groups, the high HIF-1 α score group exhibited highest enrichment of multiple oncogenic pathways, such as TNF- α signaling via NF- κ B, IL6-JAK-STAT3 signaling, mTORC1 signaling, MYC signaling, Hedgehog signaling. Notably, higher HIF-1 α scores correlated with advanced immunosuppressive TME. Besides, tumors with high HIF-1 α scores represented high non-response rate to transcatheter arterial chemoembolization (TACE) and immune checkpoint blockade (ICB). In conclusion, we developed a novel HIF-1 α score system to distinguish HCC with different degree of hypoxia and immune infiltration profiles.

Keywords: Hepatocellular carcinoma, HIF-1 α , Hypoxia, Immune checkpoint blockade, Overall survival, Transcatheter arterial chemoembolization, Immune infiltration

Introduction

Hepatocellular carcinoma (HCC), as one of the most common and lethal tumors, ranks the third leading cause of cancer-related death around the world, with an overall 5-year survival rate less than 20% [1, 2]. Presently, the major treatments for HCC include surgical resection, microwave ablation, transcatheter arterial chemoembolization (TACE),

targeted therapy with sorafenib or lenvatinib, immune checkpoint blockade (ICB), and liver transplantation [3, 4]. Despite the increasing improvements in early diagnosis and treatment in HCC, the survival of patients with HCC remains disappointed, due to the tumor heterogeneity and specific tumor microenvironment (TME) [5–8]. Besides, the conventional clinicopathological parameters, such as histologic grade, TNM stage and vascular invasion, have limited predictive power for the clinical outcome of HCC patients, due to the complex molecular mechanisms of tumor regulation [9, 10]. Thus, it is necessary to explore the potential mechanisms underlying tumor development and progression for designing more individualized treatment options for HCC.

Hypoxia and desmoplasia are the key characteristic features of HCC, in which tumor desmoplasia accelerates hypoxia, and aggravated hypoxia activates stromal cells, such as cancer stem cells and hepatic stellate cells, resulting in severe desmoplasia [11–15]. Hypoxia-inducible factor-1 α (HIF-1 α), as a chief hypoxic regulator, plays an important role for the malignant phenotypes of HCC [16–20]. For instance, HIF-1 α was found to promote the tumor progression, epithelial-mesenchymal transition, and vasculogenic mimicry formation by upregulate the expression of LOXL2 in HCC [19]. Besides, the hypoxic TME of HCC enhances the expression and function of HIF-1 α targets (e.g. MDR1, GLUT-1 and VEGF) through stabilizing HIF-1 α protein, thereby conferring sorafenib resistance in HCC [20]. Importantly, HIF-1 α impairs anti-tumor immunity by increasing CD47 or PD-L1 expression, therefore leading to an immunosuppressive TME [21–24]. Consequently, HIF-1 α may influence various cancer cell behaviors by regulator different genes expression. And several hypoxia-derived signatures have been reported to predict survival and therapeutic response of malignancy patients [25, 26], but it still remains further exploration whether hypoxia-induced HIF-1 α -related genes could be an ensemble to divide HCC patients into different clusters with various clinical outcomes, genomic alteration, oncogenic pathway and therapeutic responses. Therefore, it is of great significance to construct a HIF-1 α -specific prognostic model for assessing the molecular features of HCC with various hypoxia status.

In this study, using a series of bioinformatics and machine learning methods, HCC patients were classified into three subgroups according to HIF-1 α related genes. And an HIF-1 α score system based on the HIF-1 α cluster was established for prognostic stratification in HCC. Then, the predictive powers of our model were respectively assessed through the C-indexes and ROC analysis. Furthermore, we also systematically investigated the oncogenic pathways, immune infiltration profile, and therapeutic response to TACE and ICB for HCC in different HIF-1 α score groups.

Methods

Data processing

The mRNA expression profiles and corresponding clinical information of HCC patients were extracted from the Cancer Genome Atlas (TCGA, <https://cancergenome.nih.gov/>), the Gene Expression Omnibus (GEO, <https://www.ncbi.nlm.nih.gov/geo/>), and International Cancer Genome Consortium (ICGC, <https://icgc.org/>) databases. The raw counts of RNA-seq data from TCGA and ICGC HCC cohorts were normalized and $\log_2(x+1)$ transformed. The dataset GSE14520 involves two independent microarray datasets (e.g. GSE14520–GPL571 and GSE14520–GPL3931), which were subsequently integrated

into one cohort and proceeded for batch normalization using R packages “sav” and “limma”. Of the 371 HCC cases in the TCGA cohort, 343 were cases with overall survival (OS) longer than one month, and were enrolled in the subsequent survival analyses. And genes with zero expression levels in >50% of the tumor samples or genes with average expression <5 were excluded. The TCGA HCC cohort was used as the training set because it is an independent RNA-seq dataset with an appropriate sample size. And the RNA-seq data from GSE14520 cohort (validation cohort 1; N=242) and the ICGC cohort (validation cohort 2; N=229) were extracted for prognostic stratification validation. In addition, GSE104580 cohort (response: N=81; non-response: N=66) was used for the evaluation of therapeutic response to TACE. All datasets are freely available as public resources. Therefore, local ethics approval was not required.

Consensus clustering analysis based on HIF-1 α related genes in HCC

A total of 16 HIF-1 α related genes were selected based on previous studies [27]. The prognostic values of these HIF- α related genes were investigated in the TCGA cohort, using Kaplan–Meier (KM) survival analysis. Subsequently, using R package ‘ConsensusClusterPlus’, Partitioning Around Medoids (PAM) algorithm was performed on the selected HIF-1 α related genes to identify robust clusters of HCC, and the detail settings for clustering were shown as followed: the PAM clustering with up to 9 clusters; number of repetitions=1000 bootstraps; pFeature=1 (resampling 100% of any genes); pItem=0.8 (resampling 80% of any tumor sample) and distance=euclidean. Then, the numbers of clustering was determined by three factors, including the consensus matrices, a consensus cumulative distribution function (CDF) curve and Calinski-Harabasz Index. Besides, the different clusters were also visualized in 3-dimension by principal component analysis (PCA). Then, the OS differences among different HIF-1 α clusters were assessed by KM survival curves, and log-rank test p value were calculated. The R package ‘pheatmap’ was used to visualize HIF-1 α related genes expressions among different HIF-1 α clusters. The association between HIF-1 α clusters and clinicopathological characteristics (e.g. histologic grade, TNM stage, and vascular invasion) was assessed using the Fisher’s exact test or chi-square test. Under the threshold of $|\log_2$ fold change (FC)|>1 and $P<0.05$, differentially expressed genes between different HIF-1 α clusters were determined with the help of the R package ‘limma’. Then, the overlapping differentially expressed genes (ODEGs) were extracted for further analysis.

Establishment and validation of the HIF-1 α score system

Univariate Cox regression analysis was employed to assess the prognostic values of the ODEGs in the TCGA cohort. Then, LASSO regression analysis was conducted to determine the robust prognostic ODEGs, based on which an HIF-1 α score system was subsequently constructed. The HIF-1 α score= \sum the robust prognostic ODEGs expressions \times the corresponding coefficients of multivariable Cox regression analysis. For external validation, the HIF-1 α scores were also calculated for GSE14520 cohort and the ICGC cohort.

KM survival curve for the HIF-1 α score system was also generated based on the optimal cutoff points from the X-tile (3.6.1) [28]. The predictive capabilities of the HIF-1 α score system were assessed by ROC analysis and C-index. Besides, PCA was also

conducted to assess the prognostic stratification ability. The correlations between the HIF-1 α score system and clinicopathological parameters (e.g. TNM stage, vascular invasion, and histologic grade) were investigated using the chi-square test. Kruskal–wallis test or Wilcoxon test was utilized to assess the differences of HIF-1 α score among different groups of these clinicopathological characteristics. In addition, with the help of R package “Survival ROC”, the ROC curves were generated for the HIF-1 α score system and clinicopathological characteristics to compare their predictive discrimination for 1-, 3-, and 4-year OS.

Gene set variation analysis (GSVA)

The R package ‘gsva’ was applied to conduct GSVA to estimate the enrichment levels of 50 hallmark gene sets extracted from the Molecular Signature Database (<https://www.gsea-msigdb.org/gsea/msigdb/collections.jsp#C5>) in the TCGA cohort [29]. In addition, GSVA was also conducted to estimate the enrichment levels of 18 immunologic signatures obtained from previous studies [30, 31].

Association between the HIF-1 α score and previously reported hypoxia scores

A total of three previously reported hypoxia scores based on the TCGA cohort were downloaded from the cBioportal database (<http://www.cbioportal.org/>), including Buffa, Winter, and Ragnum hypoxia scores [32–34]. The differences in these three hypoxia scores among these three HIF-1 α score groups were then investigated. Pearson correlation analysis was used to evaluate the association between the HIF-1 α score and these three hypoxia scores. KM survival analyses were conducted for these three hypoxia scores in the TCGA cohort. In addition, ROC analyses were conducted to compare their predictive discrimination for 1-, 3-, and 4-year OS.

Statistical analysis

The SPSS 25.0 software (SPSS Inc., Chicago, IL), R software version 4.0.5 and GraphPad Prism 8.0 software (GraphPad Software, Inc.) were used for all statistical analyses. The Kaplan–Meier method with log-rank test was performed to describe patients’ survival. Variables associated with survival were determined by univariate Cox regression analysis. Significant variables in univariate Cox regression analysis were further involved in LASSO regression analysis and multivariable Cox regression analysis. Kruskal–wallis or Wilcoxon tests was used to evaluated group differences, which were expressed as means \pm standard deviation (SD). And correlation analyses were conducted using Pearson correlation coefficient. All statistical test were two-sided, and p value less than 0.05 was regarded as statistically significant.

Results

Three HIF-1 α clusters of HCC based on consensus clustering analysis

Of 16 known HIF-1 α related genes, 15 were notably correlated with worse OS of HCC patients in the TCGA cohort, including HIF1A, ALDOA, ENO1, ALDOC, PKM, HK1, GAPDH, PFKFB3, HK2, PDK1, SLC2A1, LDHA, PGK1, BNIP3, and SLC2A3 (Fig. 1A). Then PAM clustering were employed based on these 16 HIF-1 α related genes to divide HCC samples into subgroups. A 3-cluster was selected as an

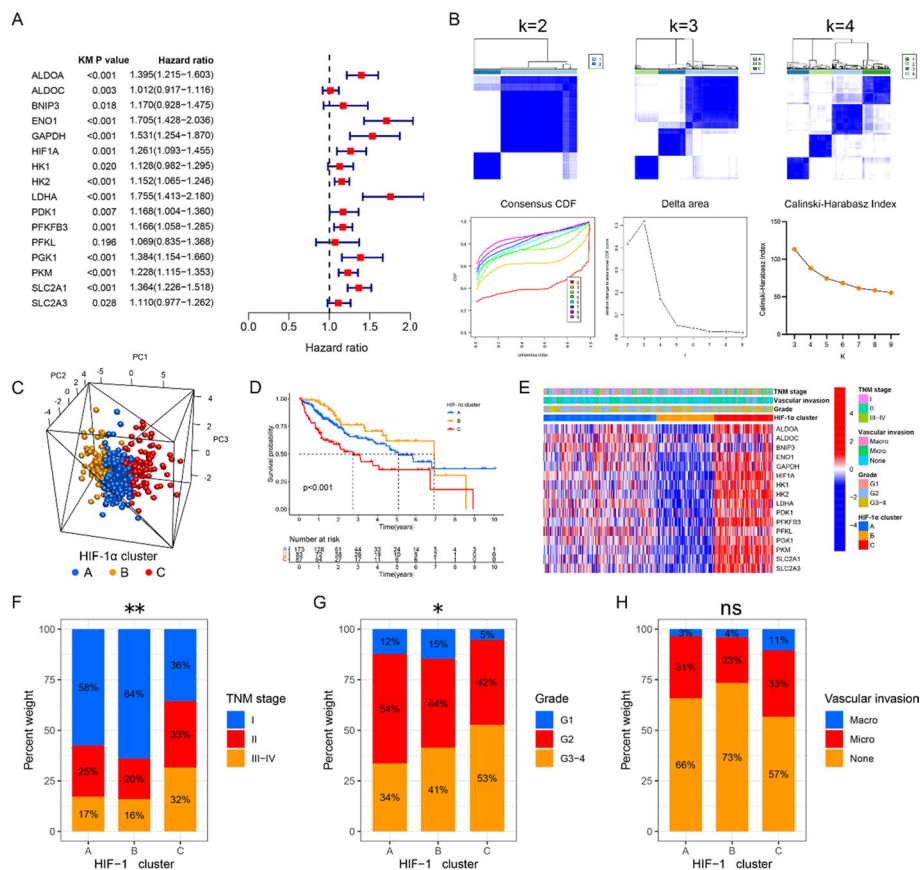


Fig. 1 Consensus clustering based on HIF-1 α related genes divided HCC samples into three clusters. **A** KM survival analyses for the selected HIF-1 α -related genes were exhibited in forest plot. **B** Subgroups are identified based on the selected HIF-1 α -related genes in TCGA HCC cohort by PAM consensus clustering upon their expression levels. Consensus clustering was based on 1000 resampled datasets and k was tested from 2 to 9. Consensus matrices, as well as the consensus cumulative distribution function (CDF) curve, delta area (change in CDF area) plot and Calinski-Harabasz Indexes are shown. **C** 3D PCA based on HIF-1 α cluster exhibited a significant spatial separation of tumor samples. **D** The KM survival curve for OS showed a significant difference among these three HIF-1 α clusters. **E** Heatmap for the 16 HIF-1 α related genes expression and clinicopathological characteristics in different HIF-1 α clusters. **F-H** HIF-1 α cluster was significantly associated with TNM stage (**F**) and histologic grade (**G**), but not vascular invasion (**H**)

appropriate solution for the consensus matrix with k=3 or k=4 deemed to be a cleanest separation among clusters, but the CDF curve and delta plot showed limited increase in area for k=3 compared to k=4. In addition, the Calinski-Harabasz Index for k=3 was larger than k=4 (Fig. 1B). According to the evidence above, the TCGA HCC samples were clustered into three groups by the selected HIF-1-related genes. 3D PCA further exhibited a significant spatial separation of tumor samples, which actually to some extent suggest that the selected HIF-1-related genes worked well in tumor sample clustering (Fig. 1C). The KM survival analysis showed significant differences in OS among these three clusters, in which HIF-1 α cluster C exhibited the best survival and HIF-1 α cluster B the worst (Fig. 1D). And a heatmap was performed to visualize the distribution of TNM stage, histologic grade, vascular invasion and the expression of these HIF-1 α -related genes in different HIF-1 α clusters (Fig. 1E).

In addition the HIF-1 α cluster was notably correlated with TNM stage and histologic grade, though not significantly associated with vascular invasion (Fig. 1F–H).

Establishment and validation of the HIF-1 α score system

The DEGs between various HIF-1 α clusters were shown by volcano plots (Additional file 1: Fig. S1A–C; Additional file 2: Table S1). And 597 ODEGs were identified among these three HIF-1 α clusters (Additional file 1: Fig. S1D). And 317 ODEGs were notably correlated with HCC patients survival ($P < 0.05$) (Additional file 3: Table S2). Furthermore, nine robust prognostic ODEGs were identified by LASSO regression analysis (Fig. 2A, B), the KM survival analyses of which were shown in Fig. 2C. tenfold cross-validation was used to overcome over-fitting effect, and an optimal λ value of 0.059 was selected. Then, using multivariable Cox regression analysis, we established an HIF-1 α score system based on these nine robust prognostic ODEGs in the TCGA cohort (training cohort), which was calculated as followed: HIF-1 α score = (0.181207 \times ADAMTS5 expression) + (0.004134 \times EGLN3 expression) + (0.074128 \times HOMER1 expression) + (0.087261 \times LPCAT1 expression) + (0.143817 \times NEIL3 expression) + (0.012743 \times PFN2 expression) + (0.107185 \times S100A9 expression) + (0.028619 \times SLC1A5 expression) + (0.014439 \times SPP1 expression). Then, patients were classified into low-, medium-, and high-HIF-1 α score groups according to the most appropriate cutoff points [28]. The low-HIF-1 α score group exhibited the best OS, and the high-HIF-1 α score group the worst (Fig. 3A). Then, for external validation, we further calculated the HIF-1 α scores respectively for the GSE14520 and ICGC cohorts. Of note, the results of KM survival analyses in the validation cohorts were consistent with that in the training cohort (Fig. 3B, C).

The HIF-1 α score system showed a reliable accuracy of survival prediction, with a C-index of 0.736 (95%CI 0.691–0.781) in the TCGA cohort, 0.614 (95%CI 0.559–0.669) in the GSE14520 cohort and 0.668 (95%CI 0.582–0.754) in the ICGC

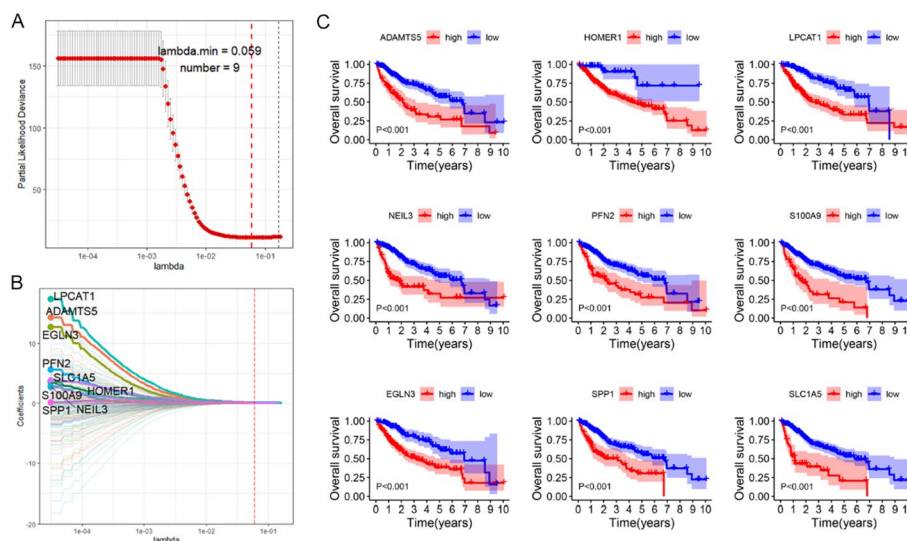


Fig. 2 Identification of nine robust prognostic ODEGs for HCC. **A, B** LASSO regression analysis identified nine robust prognostic ODEGs for HCC. **C** KM survival analysis of the nine robust prognostic ODEGs

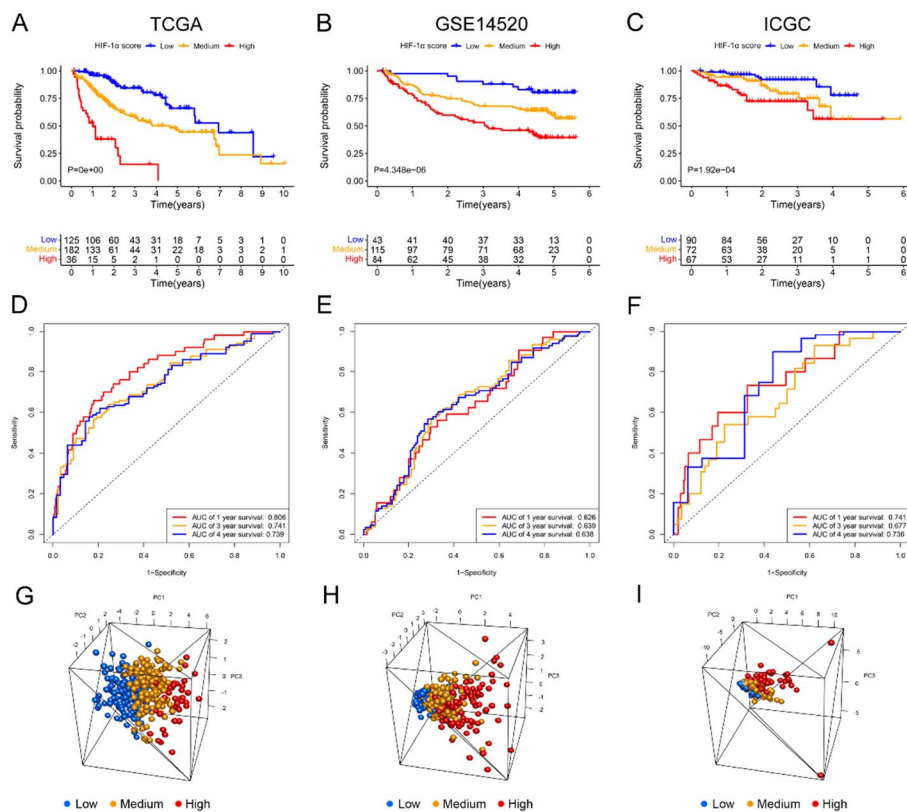


Fig. 3 Establishment and validation of an HIF-1α score system based on the HIF-1α cluster. **A–C** KM survival curves for the OS of HCC patients in different HIF-1α score groups in the TCGA (**A**), GSE14520 (**B**), and ICGC (**C**) cohorts. **D–F** ROC curve analysis of the HIF-1α score system for 1-, 3-, and 4-year OS prediction in the TCGA (**D**), GSE14520 cohort (**E**), and ICGC (**F**) cohorts. **G–I** PCA to confirm the cluster efficacy of the HIF-1α score system in the TCGA (**G**), GSE14520 (**H**), and ICGC (**I**) cohorts

cohort. Notably, the AUC values of the HIF-1α score for 1-, 3-, and 4-year OS prediction were 0.806, 0.741, and 0.739 in the TCGA cohort, 0.623, 0.639, and 0.638 in the GSE14520 cohort, and 0.741, 0.677, and 0.736 in the ICGC cohort, respectively (Fig. 3D–F). Besides, 3D PCA based on the HIF-1α score system further exhibited a significant spatial separation of tumor samples (Fig. 3G–I). These findings determined a significant predictive capability of the HIF-1α score system for HCC patients’ survival.

Association between HIF-1α score and clinicopathological features in HCC

The HIF-1α score system notably associated with advanced TNM stage, histologic grade and vascular invasion in HCC (Fig. 4A–C). Significant differences of HIF-1α scores were found among different groups of clinicopathological characteristics in HCC (Fig. 4D–F). Moreover, the HIF-1α score system was also identified as an independent prognostic factor in HCC (Fig. 4G, H). Of note, the AUC values of the HIF-1α score system for 1-, 3-, and 4-year OS were higher than TNM stage, histologic grade, and vascular invasion (Fig. 4I–K).

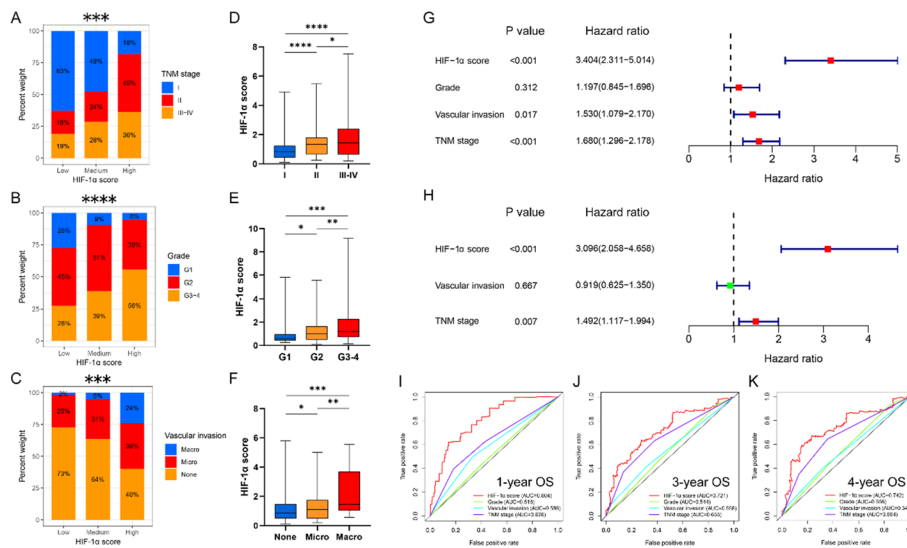


Fig. 4 The HIF-1α score system significantly associated with clinicopathological characteristics in HCC. **A–C** The HIF-1α score system significantly correlated with advanced TNM stage (**A**), histologic grade (**B**) and vascular invasion (**C**) in HCC. **D–F** Significant differences of HIF-1α score were found among HCC patients with different TNM stage (**D**), histologic grade (**E**), and vascular invasion (**F**). **G** Univariate Cox regression analysis showed that the HIF-1α score system, TNM stage, and vascular invasion were prognostic factors for HCC patients’ survival. **H** Multivariate Cox regression analysis showed that the HIF-1α score system and TNM stage were independent unfavorable prognostic factors for HCC patients’ survival. (**I–K**) ROC curves analysis for 1-, 3-, and 4-year OS prediction based on the HIF-1α score system, TNM stage, histologic grade, and vascular invasion

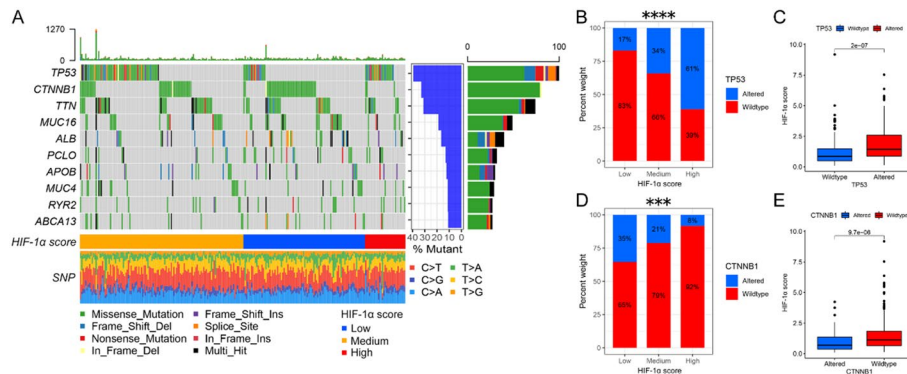


Fig. 5 Association between HIF-1α score system and somatic mutation in HCC. **A** The top 10 most commonly mutated genes in HCC patients. **B** The HIF-1α score system significantly correlated with TP53 mutation. **C** TP53 altered HCC exhibited Higher HIF-1α score. **D** HIF-1α score system significantly correlated with CTNNB1 mutation. **E** CTNNB1 altered HCC exhibited Lower HIF-1α score

Association between the HIF-1α score system and genomic mutation

Consistent with published studies, we also found that mutations in TP53, TTN, CTNNB1, MUC4, MUC16, ALB, APOB, RYR2, PCLO, and ABCA13 are the top 10 genetic alterations in HCC (Fig. 5A) [35]. Missense mutation was the most common type of genetic alteration (Fig. 5A). And the C > T transversion was the most common nucleotide change (Fig. 5A). In addition, TP53 and CTNNB1 alterations notably associated with the HIF-1α score system (Fig. 5A). TP53 alteration was significantly

correlated with higher HIF-1 α score, while CTNNB1 alteration lower HIF-1 α score (Fig. 5B–E).

Analysis of functional annotations among different HIF-1 α score groups

The differentially enriched oncologic pathways among different HIF-1 α score groups were shown in Additional file 4: Table S3. And 27 differential oncologic pathways were found overlapped among these three HIF-1 α score groups (Fig. 6A). Of note, the high HIF-1 α score group exhibited the highest enrichment levels for hypoxia-related terms (e.g. hypoxia and glycolysis), immune-related processes (e.g. inflammatory response, IL2-STAT5 signaling, TNF- α signaling via NF- κ B, IL6-JAK-STAT3 signaling, allograft rejection, and complement), crucial oncogenic pathways (e.g. mTORC1, MYC, PI3K-AKT-mTOR, and Hedgehog signalings), and proliferation processes (e.g. G2M checkpoint, E2F targets, mitotic spindle), while the low HIF-1 α score group the lowest. However, metabolic processes (e.g. oxidative phosphorylation, xenobiotic metabolism, bile acid metabolism, and peroxisome), on the contrary, were notably suppressed in tumors with HIF-1 α scores, but markedly enriched in tumors with low HIF-1 α scores (Fig. 6A).

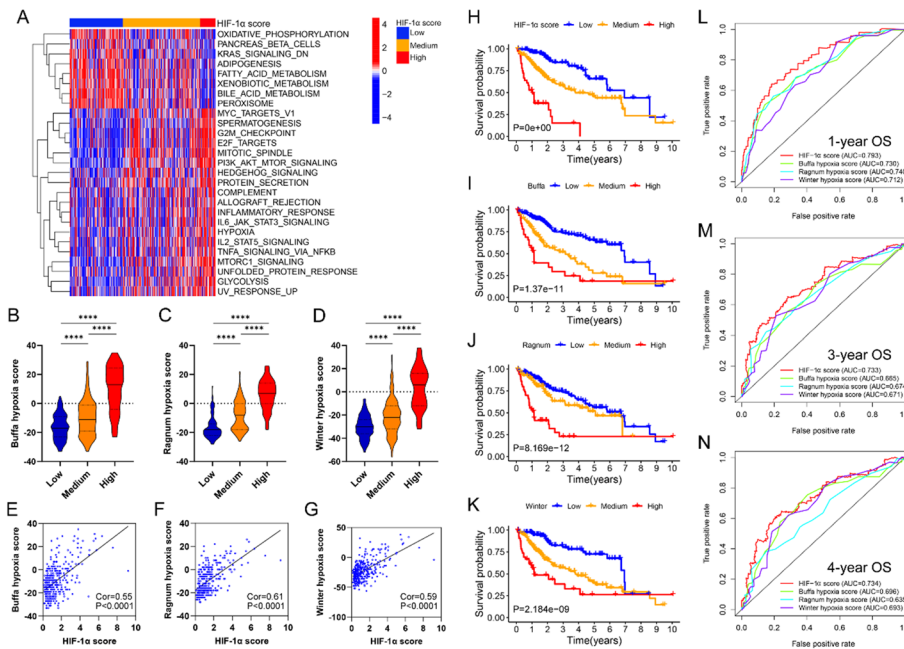


Fig. 6 Association between HIF-1 α score and oncologic biological processes and hypoxia status in HCC. **A** Heatmap to exhibit 27 differential crucial oncologic biological pathways overlapped among the three HIF-1 α score groups. **B–D** Stepwise increasing Buffa (**B**), Ragnum (**C**), and Winter (**D**) hypoxia scores were found from low to high HIF-1 α score group. **E–G** HIF-1 α score significantly associated with Buffa (**E**), Ragnum (**F**), and Winter (**G**) hypoxia score systems. **H–K** KM survival curves for OS of HCC patients according to the HIF-1 α (**H**), Buffa (**I**), Ragnum (**J**), and Winter (**K**) score systems in the TCGA cohort. **L–N** ROC curves for 1- (**L**), 3- (**M**), and 4- (**N**) year OS prediction based on the HIF-1 α , Buffa, Ragnum, and Winter score systems in the TCGA cohort

Comparison of our HIF-1 α score system with other previously reported hypoxia score systems

Of note, stepwise increasing Buffa, Winter and Ragnum hypoxia scores were observed from low to high HIF-1 α score groups (Fig. 6B–D). These findings verified our HIF-1 α score system a reflection of the hypoxia status in HCC. Besides, the HIF-1 α score system notably associated with these previous reported hypoxia score systems (Buffa: Cor=0.55, $P < 0.0001$; Ragnum: Cor=0.61, $P < 0.0001$; Winter: Cor=0.59, $P < 0.0001$) (Fig. 6E–G). Compared with these previously reported hypoxia score system, KM survival analyses indicated that our HIF-1 α score system exhibited the best stratification ability of prognosis (Fig. 6H–K). In addition, the ROC analyses also suggested that the HIF-1 α score system possessed the optimal predictive capability for 1-, 3-, and 4-year survival in HCC (Fig. 6L–N). Taken together, these findings suggested the superior predictive value of the HIF-1 α score system for patient prognoses.

Tumors with high HIF-1 α scores were associated with high non-response rate to TACE

GSE104580 cohort was utilized to investigate the predictive capability of the HIF-1 α score system for therapeutic response to TACE. Then, stepwise increasing portions of TACE-non-response HCC patients were found from low to high HIF-1 α score groups (Fig. 7A). Higher HIF-1 α scores were found in TACE-non-responsive tumors when compared with TACE-responsive tumors (Fig. 7B). Besides, we evaluated the predictive capability of the HIF-1 α score system for therapeutic response to TACE, the AUC of which was 0.793 (95%CI 0.719–0.868) ($P < 0.0001$) (Fig. 7C). These findings suggested that the HIF-1 α score system performed well in the prediction of therapeutic response to TACE.

Tumors with high HIF-1 α scores correlated with immunosuppressive phenotype and high non-response rate to immune checkpoint blockade

The 18 immune-related signatures were shown in Fig. 8A, including macrophages, neutrophils, myeloid-derived suppressor cells (MDSC), gamma delta T cells, regulatory T cells (Tregs), T follicular helper cells, plasmacytoid dendritic cells, activated dendritic cells, immature dendritic cells, immature B cell, activated B cell, natural

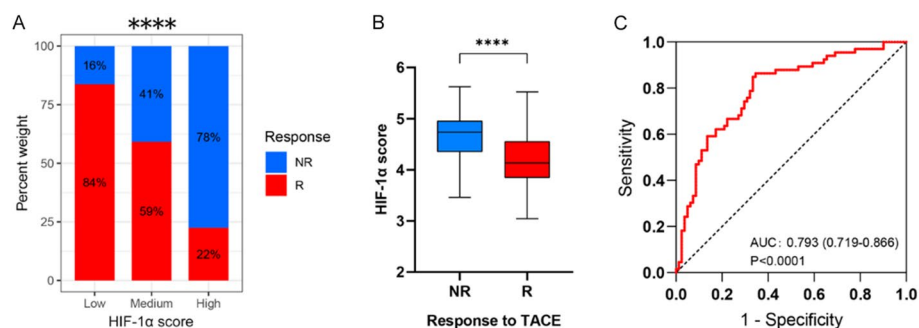


Fig. 7 Tumors with high HIF-1 α score exhibited high non-response rate to TACE. **A** Stepwise increasing portions of TACE-non-response HCC patients were found from low to high HIF-1 α score groups. **B** Higher HIF-1 α scores were found in TACE-non-responsive tumors when compared with TACE-responsive tumors. **C** ROC curve analysis to assess the diagnostic capability of the HIF-1 α score system for the prediction of therapeutic response to TACE

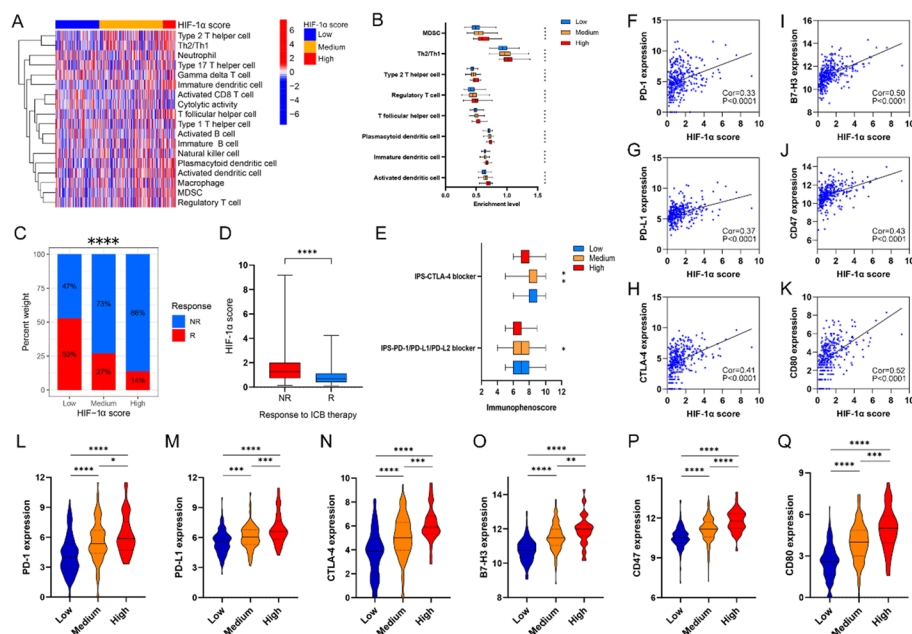


Fig. 8 Tumors with high HIF-1 α score notably associated with immunosuppressive phenotype and high non-response rate to immune checkpoint blockade. **A** Heatmap to exhibit the 18 immune-related terms in the three HIF-1 α score groups. **B** Enrichment levels of MDSC, Tregs, Th2 cells, T follicular helper cells, and dendritic cells (Plasmacytoid, immature, and activated) in the three HIF-1 score groups. **C** Stepwise increasing portions of ICB-non-response HCC patients were found from low to high HIF-1 α score groups. **D** Higher HIF-1 α scores were found in ICB-non-responsive tumors when compared with ICB-responsive tumor. **E** The IPS-CTLA-4 and IPS-PD-1/PD-L1/PD-L2 were significantly lowest in patients in the high HIF-1 α score group. **F–K** Higher HIF-1 α scores significantly associated with higher PD-1 (**F**), PD-L1 (**G**), CTLA-4 (**H**), B7-H3 (**I**), CD47 (**J**), and CD80 (**K**) expressions in HCC. **L–Q** Tumors in high HIF-1 α score group exhibited highest expressions of PD-1 (**L**), PD-L1 (**M**), CTLA-4 (**N**), B7-H3 (**O**), CD47 (**P**), and CD80 (**Q**), while those in the low-HIF-1 α score group exhibited the lowest

killer cells, cytolytic activity, activated CD8⁺ T cells, type 17 T-helper cells (Th17 cells), type 1 T-helper cells (Th1 cells), type 2 T-helper cells (Th2 cells), and Th2/Th1. Stepwise increasing infiltrations of pro-tumor immune cells were observed from low to high HIF-1 α score groups, including MDSC, Tregs, Th2 cells, T follicular helper cells, and dendritic cells (Plasmacytoid, activated and immature) (Fig. 8B). In addition, tumors with high HIF-1 α score possessed increased enrichment level of Th2/Th1 (Fig. 8B).

Then, ImmuneCellAI (<http://bioinfo.life.hust.edu.cn/ImmCellAI/#/>) was utilized for the prediction of therapeutic response to immune checkpoint blockade (ICB) [36]. Stepwise increasing portions of ICB-non-response HCC patients were found from low to high HIF-1 α score groups (Fig. 8C). Higher HIF-1 α scores were found in ICB-non-responsive tumors when compared with ICB-responsive tumors (Fig. 8D). To further verify the predictive ability of HIF-1 α score system in patients' response to ICB, we investigated the differences in immunophenoscore (IPS) among various HIF-1 α score groups, which was obtained from the Cancer Immunome Atlas (<https://tcia.at/>) and used to predict the efficacy of ICB [37]. Two subtypes of IPS, including IPS-CTLA-4 and IPS-PD-1/PD-L1/PD-L2, were selected for further analysis as the surrogates of HCC patients' response to anti-CTLA-4 and anti-PD-1/PD-L1/PD-L2

treatment. The IPS-CTLA-4 and IPS-PD-1/PD-L1/PD-L2 were significantly lowest in patients in the high HIF-1 α score group (Fig. 8E). Besides, HIF-1 α scores positively correlated with PD-1, PD-L1, CTLA-4, B7-H3, CD47, and CD80 expressions, which are crucial for the immunosuppressive phenotype (Fig. 8F–K) [38–43]. And tumors with high HIF-1 α score possessed increased expressions of PD-1, PD-L1, CTLA-4, B7-H3, CD47, and CD80 (Fig. 8L–Q). Taken together, our findings suggest an immunosuppressive status and high non-response rate to ICB in tumors with high HIF-1 α score, identifying the HIF-1 α score system as a potential indicator of the immunogenic profiles in HCC.

Discussion

The current study classified HCC patients in the TCGA cohort into three HIF-1 α clusters based on the 16 reported HIF-1 α related genes. Then, we also established an HIF-1 α score system based on nine prognostic ODEGs among various HIF-1 α clusters, which exhibited satisfactory predictive capability for survival. Furthermore, compared with other previous hypoxia score systems, our model possessed the optimal predictive efficacy for OS in HCC. Putting these together, we constructed a novel HIF-1 α score system for HCC, which works well in prognostic prediction and hypoxic status evaluation of HCC patients.

Some of the nine genes involved in the HIF-1 α score system have been reported to play crucial roles in liver carcinogenesis. Previous study by Zhu et al. demonstrated that ADAMTS5 is an unfavorable prognostic biomarker with a potential role in extracellular matrix remodeling and metabolic regulation in HCC, and could be a promising therapeutic target for patients with HCC [44]. HOMER1 was identified as an unfavorable prognostic biomarker associated with glycolysis in HCC, but its potential oncologic role in HCC still remains further works [45]. LPCAT1 overexpression promotes the malignant phenotypes of HCC through directly inhibiting STAT1 [46]. NEIL3 overexpression enables the repair of oxidative DNA damage at telomeres in mitosis, which is critical to prevent senescence of HCC cells [47]. The oncologic role of PFN2 has been reported in various malignancies, but little is known in HCC, and for the first time, we identified PFN2 as a novel unfavorable prognostic biomarker in HCC [48–51]. Upregulation of S100A9 by HBx-mediated NF- κ B activation promotes tumor progression in HCC [52]. Notably, it has been reported that the EGLN3 is recruited by HIF1A to crosstalk with PKM2, thereby enhancing HIF-1 α transactivation [53]. SPP1 overexpression promotes HCC progression and metastasis by activating CCR1 expression via the PI3K-AKT-HIF-1 α signaling pathway [54]. SLC1A5 is a critical glutamine transporter in malignancies, and activation of which captures huge amounts of glutamine [55, 56]. It should be noted, based on data mining, that all the nine genes utilized in this model should be HIF-1 α related genes, though most of which have not been found to be modulated by HIF-1 α . Therefore, further works should be conducted to explore how HIF-1 α modulates or interacts with these genes.

In this study, HCC with high HIF-1 α scores are considered much more aggressive, due to the notable associations with shorter OS, more advanced TNM stage, histologic grade and vascular invasion. By investigating the functional annotations among HIF-1 α high, medium, and low score tumors, MYC signaling, mTORC1 pathway, and Hedgehog

signaling were found significantly enriched in tumor with high HIF-1 α score. MYC has been reported to be one of the major drivers of HCC initiation and progression [57, 58]. MYC-upregulated tumor cells were found to have enhanced glucose and glutamine utilization and overexpression of critical glycolytic and glutaminolytic enzymes [59–61]. And mTORC1 pathway has also been identified as a critical oncogenic signaling pathway for tumor cell growth, survival, and metabolism [62–64]. Notably, mTORC1 pathway has been found to enhance the transcription and translation of HIF-1 α , and could serve as a central activator of the hypoxia response (e.g. Warburg effect) by inducing multiple signaling pathways [65–67]. Sun et al. also demonstrated that dual inhibition of both mTOR and glycolysis synergistically impairs the proliferation and tumorigenesis of mTOR hyperactive cells [68]. Hedgehog signaling facilitates the metastasis and drug resistance of HCC in combination with other oncogenic pathways, such as MYC pathway and TGF- β signaling [69–71]. Taken together, these findings demonstrate that MYC, mTORC1 pathways, and Hedgehog signaling are crucial oncogenic drivers in high HIF-1 α score tumors, which might provide a preliminary theoretical basis for combination treatment using MYC inhibitor and HIF-1 α inhibitor, or using mTORC1 inhibitor and HIF-1 α inhibitor, or using Hedgehog signaling inhibitor and HIF-1 α inhibitor in these highly aggressive and hypoxic HCCs.

The current study indicated that the HIF-1 α score system performed well in the prediction of therapeutic response to TACE, in which tumors with high HIF-1 α score represented high non-response rate to TACE. Consistently, Wei et al. revealed that activation of HIF-1 α /pAKT loop leads to HCC non-response to TACE [72]. Moreover, previous study by Martin et al. also showed that hypoxia signaling and glycolysis-related pathways are upregulated in HCCs insensitive to TACE, and targeting PKM2, an HIF-1 α -related gene, could improve the response rate to TACE [73]. Thus, for tumors with high HIF-1 α , strategies to inhibit HIF-1 α signaling or glycolysis-related pathway may be helpful for recovering or improving the efficacy of TACE.

In addition to activation of multiple critical oncogenic pathways, we revealed that HCCs with high HIF-1 α scores were more immunosuppressive and higher non-response rate to ICB (e.g. PD-1/PD-L1 and CTLA-4 inhibition). In particular, tumors with high HIF-1 α scores possessed high pro-tumor immune cells infiltrations, especially for MDSC and Tregs. These tumors had high expression of important immune checkpoint proteins, including PD-1, PD-L1, CTLA-4, B7-H3, CD47, and CD80. Previous studies revealed that MDSCs exhibit immunosuppressive activities in TME, facilitating immune escape and non-response to ICB of tumor cells [74–77]. MDSCs were also able to facilitate the pro-tumor activities of Treg cells, thereby dampening anti-tumor immunity of effective T cells in HCC [78, 79]. Chiu et al. demonstrated that HIF-1 α increases the transcription of CCL26 in tumor cells to recruit MDSCs to the hypoxic regions of tumor [80]. Notably, tumors with high HIF-1 α scores also showed significant upregulations of TNF- α signaling via NF- κ B and IL6-JAK-STAT3 signaling, which were critical for the accumulation and immunosuppressive capacity of MDSCs [81–87]. Targeting MDSC trafficking has been reported to enhance anti-PD-1 efficacy, representing a promising therapeutic strategy against HCCs [74, 80, 82]. It is also reported that hypoxia-induced HIF-1 α upregulates PD-L1 expression in several solid tumors, which was consistent with our findings that tumors with higher HIF-1 α score exhibited higher expression PD-L1

[88]. Taken together, HCCs with high HIF-1 α scores exhibited a highly immunosuppressive TME. And low/medium HIF-1 α score tumors seem to be more suitable for immunotherapy. For highly immunosuppressive tumors, treatment strategies to restrain pro-tumor immunity by targeting HIF-1 α or suppressing desmoplasia or hypoxia may be promising for enhancing the effect of immunotherapy.

Conclusions

In conclusion, our study developed a novel HIF-1 α score system to discriminate HCC with different hypoxia status and immunogenic cold TMEs, which exhibited reliable predictive efficacy for patient prognoses, TACE therapeutic response, and immunotherapy response. Besides, our study present the distinctive functional and immunogenic profiles for tumors with high HIF-1 α scores and low/medium HIF-1 α scores, which might provide preliminary rationales for individual treatment options of these HCC patients.

Abbreviations

HCC	Hepatocellular carcinoma
OS	Overall survival
DFS	ICB: immune checkpoint blockade
TCGA	The cancer genome atlas
ICGC	International cancer genome consortium
TME	Tumor microenvironment
HIF-1 α	Hypoxia-inducible factor-1 α
ODEG	Overlapping differentially expressed gene
TACE	Transcatheter arterial chemoembolization
KM	Kaplan–Meier
GSVA	Gene set variation analysis
MDSC	Myeloid-derived suppressor cells
Th17 cells	Type 17 T-helper cells
Th1 cells	Type 1 T-helper cells
Th2 cells	Type 2 T-helper cells

Supplementary Information

The online version contains supplementary material available at <https://doi.org/10.1186/s40537-023-00752-1>.

Additional file 1. Fig. S1 (A) Differential expression analysis between HIF-1 α cluster A and B. (B) Differential expression analysis between HIF-1 α cluster A and C. (C) Differential expression analysis between HIF-1 α cluster B and C. (D) Intersection of differential expressed genes among these three HIF-1 α clusters.

Additional file 2. Table S1. Differentially expressed genes between various HIF-1 α clusters.

Additional file 3. Table S2. Univariable Cox regression analysis identified 317 prognostic ODEGs for patients with HCC.

Additional file 4. Table S3. The differential biological pathways between different HIF-1 α score groups.

Acknowledgements

The authors would like to give their sincere appreciation to the reviewers for their helpful comments on this article and research groups for the TCGA, ICGC and GEO, which provided data for this collection.

Author contributions

Z-HK, S-CZ and C-YJ designed the study. Z-HK, Z-ZD, C-B, T-CW, C-XM, T-WL, Y-L, X-ZQ, W-QB, M-XW and W-BK obtained and assembled data. Z-HK, Z-ZD, C-B and T-CW analyzed and interpreted the data. Z-HK, Z-ZD and C-B wrote the manuscript, which was edited by all authors, who have approved the final version for submission. All authors read and approved the final manuscript.

Funding

This study was supported by National Natural Science Foundation of China (project NO.: 81972263, 82072714, and 82103221), the program of Guangdong Provincial Clinical Research Center for Digestive Diseases (2020B111170004), China Postdoctoral Science Foundation (2020M683094), the Guangdong Basic and Applied Basic Research Foundation (2022A1515011599) and the Excellent Young Talent Program of Guangdong Provincial People's Hospital (KY012021190).

Availability of data and materials

All data generated and described in this article are available from the corresponding web servers, and are freely available to any scientist wishing to use them for noncommercial purposes, without breaching participant confidentiality. Further information is available from the corresponding author on reasonable request.

Declarations

Ethics approval and consent to participate

Not applicable.

Consent for publication

All authors have reviewed the manuscript and consented for publication.

Competing interests

The authors declare that they have no competing interests.

Received: 26 July 2022 Accepted: 8 May 2023

Published online: 22 May 2023

References

1. Villanueva A. Hepatocellular carcinoma. *N Engl J Med*. 2019;380:1450–62. <https://doi.org/10.1056/NEJMra1713263>.
2. Nault JC, Villanueva A. Biomarkers for hepatobiliary cancers. *Hepatology*. 2021. <https://doi.org/10.1002/hep.31175>.
3. Hartke J, Johnson M, Ghabril M. The diagnosis and treatment of hepatocellular carcinoma. *Semin Diagn Pathol*. 2017;34:153–9. <https://doi.org/10.1053/j.semdp.2016.12.011>.
4. Wang C, Vegna S, Jin H, Benedict B, et al. Inducing and exploiting vulnerabilities for the treatment of liver cancer. *Nature*. 2019;574:268–72. <https://doi.org/10.1038/s41586-019-1607-3>.
5. Gao Q, Wang XY, Zhou J, Fan J. Heterogeneity of intermediate-stage HCC necessitates personalized management including surgery. *Nat Rev Clin Oncol*. 2015;12:10. <https://doi.org/10.1038/nrclinonc.2014.122-c1>.
6. Gao Q, Wang XY, Zhou J, Fan J. Multiple carcinogenesis contributes to the heterogeneity of HCC. *Nat Rev Gastroenterol Hepatol*. 2015;12:13. <https://doi.org/10.1038/nrgastro.2014.6-c1>.
7. Bruix J, da Fonseca LG, Reig M. Insights into the success and failure of systemic therapy for hepatocellular carcinoma. *Nat Rev Gastroenterol Hepatol*. 2019;16:617–30. <https://doi.org/10.1038/s41575-019-0179-x>.
8. Farzaneh Z, Vosough M, Agarwal T, Farzaneh M. Critical signaling pathways governing hepatocellular carcinoma behavior; small molecule-based approaches. *Cancer Cell Int*. 2021;21:208. <https://doi.org/10.1186/s12935-021-01924-w>.
9. Wang Z, Pan L, Guo D, Luo X, et al. A novel five-gene signature predicts overall survival of patients with hepatocellular carcinoma. *Cancer Med*. 2021;10:3808–21. <https://doi.org/10.1002/cam4.3900>.
10. Bruix J, Reig M, Sherman M. Evidence-based diagnosis, staging, and treatment of patients with hepatocellular carcinoma. *Gastroenterology*. 2016;150:835–53. <https://doi.org/10.1053/j.gastro.2015.12.041>.
11. Shao S, Duan W, Xu Q, Li X, et al. Curcumin suppresses hepatic stellate cell-induced hepatocarcinoma angiogenesis and invasion through downregulating CTGF. *Oxid Med Cell Longev*. 2019;2019:8148510. <https://doi.org/10.1155/2019/8148510>.
12. Lu Y, Lin N, Chen Z, Xu R. Hypoxia-induced secretion of platelet-derived growth factor-BB by hepatocellular carcinoma cells increases activated hepatic stellate cell proliferation, migration and expression of vascular endothelial growth factor-A. *Mol Med Rep*. 2015;11:691–7. <https://doi.org/10.3892/mmr.2014.2689>.
13. Iyer SC, Kannan A, Gopal A, Devaraj N, et al. Receptor channel TRPC6 orchestrate the activation of human hepatic stellate cell under hypoxia condition. *Exp Cell Res*. 2015;336:66–75. <https://doi.org/10.1016/j.yexcr.2015.03.023>.
14. Zhang M, Zhang W, Wu Z, Liu S, et al. Artemin is hypoxia responsive and promotes oncogenicity and increased tumor initiating capacity in hepatocellular carcinoma. *Oncotarget*. 2016. <https://doi.org/10.18632/oncotarget.6572>.
15. Caraglia M, Giuberti G, Marra M, Addeo R, et al. Oxidative stress and ERK1/2 phosphorylation as predictors of outcome in hepatocellular carcinoma patients treated with sorafenib plus octreotide LAR. *Cell Death Dis*. 2011. <https://doi.org/10.1038/cddis.2011.34>.
16. Yao B, Li Y, Niu Y, Wang L, et al. Hypoxia-induced miR-3677-3p promotes the proliferation, migration and invasion of hepatocellular carcinoma cells by suppressing SIRT5. *J Cell Mol Med*. 2020;24:8718–31. <https://doi.org/10.1111/jcmm.15503>.
17. Zeng Z, Lu Q, Liu Y, Zhao J, et al. Effect of the hypoxia inducible factor on sorafenib resistance of hepatocellular carcinoma. *Front Oncol*. 2021. <https://doi.org/10.3389/fonc.2021.641522>.
18. Zhang Q, Cheng Q, Xia M, Huang X, et al. Hypoxia-induced lncRNA-NEAT1 sustains the growth of hepatocellular carcinoma via regulation of miR-199a-3p/UCK2. *Front Oncol*. 2020;10:998. <https://doi.org/10.3389/fonc.2020.00998>.
19. Wang M, Zhao X, Zhu D, Liu T, et al. HIF-1 α promoted vasculogenic mimicry formation in hepatocellular carcinoma through LOXL2 up-regulation in hypoxic tumor microenvironment. *J Exp Clin Cancer Res*. 2017;36:60. <https://doi.org/10.1186/s13046-017-0533-1>.
20. Liang Y, Zheng T, Song R, Wang J, et al. Hypoxia-mediated sorafenib resistance can be overcome by EF24 through von hippel-lindau tumor suppressor-dependent HIF-1 α inhibition in hepatocellular carcinoma. *Hepatology*. 2013;57:1847–57. <https://doi.org/10.1002/hep.26224>.
21. You L, Wu W, Wang X, Fang L, et al. The role of hypoxia-inducible factor 1 in tumor immune evasion. *Med Res Rev*. 2021;41:1622–43. <https://doi.org/10.1002/med.21771>.

22. Noman MZ, Desantis G, Janji B, Hasmim M, et al. PD-L1 is a novel direct target of HIF-1 α , and its blockade under hypoxia enhanced MDSC-mediated T cell activation. *J Exp Med*. 2014;211:781–90. <https://doi.org/10.1084/jem.20131916>.
23. Samanta D, Park Y, Ni X, Li H, et al. Chemotherapy induces enrichment of CD47 (+)/CD73 (+)/PDL1 (+) immune evasive triple-negative breast cancer cells. *Proc Natl Acad Sci U S A*. 2018;115:E1239–48. <https://doi.org/10.1073/pnas.1718197115>.
24. Zhang H, Lu H, Xiang L, Bullen JW, et al. HIF-1 regulates CD47 expression in breast cancer cells to promote evasion of phagocytosis and maintenance of cancer stem cells. *Proc Natl Acad Sci U S A*. 2015;112:E6215–23. <https://doi.org/10.1073/pnas.1520032112>.
25. Shi R, Bao X, Unger K, Sun J, et al. Identification and validation of hypoxia-derived gene signatures to predict clinical outcomes and therapeutic responses in stage I lung adenocarcinoma patients. *Theranostics*. 2021;11:5061–76. <https://doi.org/10.7150/thno.56202>.
26. Chen D, Huang H, Zang L, Gao W, et al. Development and verification of the hypoxia- and Immune-Associated prognostic signature for pancreatic ductal adenocarcinoma. *Front Immunol*. 2021. <https://doi.org/10.3389/fimmu.2021.728062>.
27. Semenza GL. HIF-1: upstream and downstream of cancer metabolism. *Curr Opin Genet Dev*. 2010;20:51–6. <https://doi.org/10.1016/j.gde.2009.10.009>.
28. Camp RL, Dolled-Filhart M, Rimm DL. X-tile: a new bio-informatics tool for biomarker assessment and outcome-based cut-point optimization. *Clin Cancer Res*. 2004;10:7252–9. <https://doi.org/10.1158/1078-0432.CCR-04-0713>.
29. Hanzelmann S, Castelo R, Guinney J. GSEA: gene set variation analysis for microarray and RNA-seq data. *BMC Bioinformatics*. 2013;14:7. <https://doi.org/10.1186/1471-2105-14-7>.
30. Bindea G, Mlecnik B, Tosolini M, Kirilovsky A, et al. Spatiotemporal dynamics of intratumoral immune cells reveal the immune landscape in human cancer. *Immunity*. 2013;39:782–95. <https://doi.org/10.1016/j.immuni.2013.10.003>.
31. Rooney MS, Shukla SA, Wu CJ, Getz G, et al. Molecular and genetic properties of tumors associated with local immune cytolytic activity. *Cell*. 2015;160:48–61. <https://doi.org/10.1016/j.cell.2014.12.033>.
32. Buffa FM, Harris AL, West CM, Miller CJ. Large meta-analysis of multiple cancers reveals a common, compact and highly prognostic hypoxia metagene. *Br J Cancer*. 2010;102:428–35. <https://doi.org/10.1038/sj.bjc.6605450>.
33. Ragnum HB, Vlatkovic L, Lie AK, Axcrona K, et al. The tumour hypoxia marker pimonidazole reflects a transcriptional programme associated with aggressive prostate cancer. *Br J Cancer*. 2015;112:382–90. <https://doi.org/10.1038/bjc.2014.604>.
34. Winter SC, Buffa FM, Silva P, Miller C, et al. Relation of a hypoxia metagene derived from head and neck cancer to prognosis of multiple cancers. *Cancer Res*. 2007;67:3441–9. <https://doi.org/10.1158/0008-5472.CAN-06-3322>.
35. Xie F, Bai Y, Yang X, Long J, et al. Comprehensive analysis of tumour mutation burden and the immune microenvironment in hepatocellular carcinoma. *Int Immunopharmacol*. 2020. <https://doi.org/10.1016/j.intimp.2020.107135>.
36. Miao YR, Zhang Q, Lei Q, Luo M, et al. ImmuCellAI: a unique method for comprehensive T-cell subsets abundance prediction and its application in cancer immunotherapy. *Adv Sci*. 2020;7:1902880. <https://doi.org/10.1002/adv.201902880>.
37. Charoentong P, Finotello F, Angelova M, Mayer C, et al. Pan-cancer Immunogenomic analyses reveal genotype-immunophenotype relationships and predictors of response to checkpoint blockade. *Cell Rep*. 2017;18:248–62. <https://doi.org/10.1016/j.celrep.2016.12.019>.
38. Rotte A. Combination of CTLA-4 and PD-1 blockers for treatment of cancer. *J Exp Clin Cancer Res*. 2019;38:255. <https://doi.org/10.1186/s13046-019-1259-z>.
39. Ohaegbulam KC, Assal A, Lazar-Molnar E, Yao Y, et al. Human cancer immunotherapy with antibodies to the PD-1 and PD-L1 pathway. *Trends Mol Med*. 2015;21:24–33. <https://doi.org/10.1016/j.molmed.2014.10.009>.
40. Flem-Karlsen K, Fodstad O, Tan M, Nunes-Xavier CE. B7–H3 in cancer—beyond immune regulation. *Trends Cancer*. 2018;4:401–4. <https://doi.org/10.1016/j.trecan.2018.03.010>.
41. Casey SC, Tong L, Li Y, Do R, et al. MYC regulates the antitumor immune response through CD47 and PD-L1. *Science*. 2016;352:227–31. <https://doi.org/10.1126/science.aac9935>.
42. Veillette A, Chen J. SIRP α -CD47 immune checkpoint blockade in anticancer therapy. *Trends Immunol*. 2018;39:173–84. <https://doi.org/10.1016/j.it.2017.12.005>.
43. Chen R, Ganesan A, Okoye I, Arutyunova E, et al. Targeting B7–1 in immunotherapy. *Med Res Rev*. 2020;40:654–82. <https://doi.org/10.1002/med.21632>.
44. Zhu Z, Xu J, Wu X, Lin S, et al. In Silico identification of contradictory role of ADAMTS5 in hepatocellular carcinoma. *Technol Cancer Res Treat*. 2021;20:1533033820986826. <https://doi.org/10.1177/1533033820986826>.
45. Jiang L, Zhao L, Bi J, Guan Q, et al. Glycolysis gene expression profilings screen for prognostic risk signature of hepatocellular carcinoma. *Aging*. 2019. <https://doi.org/10.18632/aging.102489>.
46. Ji W, Peng Z, Sun B, Chen L, et al. LpCat1 promotes malignant transformation of hepatocellular carcinoma cells by directly suppressing STAT1. *Front Oncol*. 2021. <https://doi.org/10.3389/fonc.2021.678714>.
47. Zhao Z, Gad H, Benitez-Buelga C, Sanjiv K, et al. NEIL3 prevents senescence in hepatocellular carcinoma by repairing oxidative lesions at telomeres during mitosis. *Cancer Res*. 2021;81:4079–93. <https://doi.org/10.1158/0008-5472.CAN-20-1028>.
48. Ling Y, Cao Q, Liu Y, Zhao J, et al. Profilin 2 (PFN2) promotes the proliferation, migration, invasion and epithelial-to-mesenchymal transition of triple negative breast cancer cells. *Breast Cancer*. 2021;28:368–78. <https://doi.org/10.1007/s12282-020-01169-x>.
49. Cao Q, Liu Y, Wu Y, Hu C, et al. Profilin 2 promotes growth, metastasis, and angiogenesis of small cell lung cancer through cancer-derived exosomes. *Aging*. 2020. <https://doi.org/10.18632/aging.202213>.
50. Tang YN, Ding WQ, Guo XJ, Yuan XW, et al. Epigenetic regulation of Smad2 and Smad3 by profilin-2 promotes lung cancer growth and metastasis. *Nat Commun*. 2015;6:8230. <https://doi.org/10.1038/ncomms9230>.
51. Jiang M, Qiu N, Xia H, Liang H, et al. Long noncoding RNA FOXD2AS1/miR1505p/PFN2 axis regulates breast cancer malignancy and tumorigenesis. *Int J Oncol*. 2019;54:1043–52. <https://doi.org/10.3892/ijo.2019.4671>.

52. Duan L, Wu R, Zhang X, Wang D, et al. HBx-induced S100A9 in NF-kappaB dependent manner promotes growth and metastasis of hepatocellular carcinoma cells. *Cell Death Dis.* 2018;9:629. <https://doi.org/10.1038/s41419-018-0512-2>.
53. Zheng F, Chen J, Zhang X, Wang Z, et al. The HIF-1alpha antisense long non-coding RNA drives a positive feedback loop of HIF-1alpha mediated transactivation and glycolysis. *Nat Commun.* 2021;12:1341. <https://doi.org/10.1038/s41467-021-21535-3>.
54. Zhu Y, Gao XM, Yang J, Xu D, et al. C-C chemokine receptor type 1 mediates osteopontin-promoted metastasis in hepatocellular carcinoma. *Cancer Sci.* 2018;109:710–23. <https://doi.org/10.1111/cas.13487>.
55. Kanai Y, Hediger MA. The glutamate/neutral amino acid transporter family SLC1: molecular, physiological and pharmacological aspects. *Pflugers Arch.* 2004;447:469–79. <https://doi.org/10.1007/s00424-003-1146-4>.
56. Liu P, Ge M, Hu J, Li X, et al. A functional mammalian target of rapamycin complex 1 signaling is indispensable for c-Myc-driven hepatocarcinogenesis. *Hepatology.* 2017;66:167–81. <https://doi.org/10.1002/hep.29183>.
57. Wang H, Wang P, Xu M, Song X, et al. Distinct functions of transforming growth factor-beta signaling in c-MYC driven hepatocellular carcinoma initiation and progression. *Cell Death Dis.* 2021;12:200. <https://doi.org/10.1038/s41419-021-03488-z>.
58. Mei C, Jiang X, Gu Y, Wu X, et al. YY1-mediated reticulocalbin-2 upregulation promotes the hepatocellular carcinoma progression via activating MYC signaling. *Am J Cancer Res.* 2021;11:2238–51.
59. Shim H, Dolde C, Lewis BC, Wu CS, et al. c-Myc transactivation of LDH-A: implications for tumor metabolism and growth. *Proc Natl Acad Sci U S A.* 1997;94:6658–63. <https://doi.org/10.1073/pnas.94.13.6658>.
60. Stine ZE, Walton ZE, Altman BJ, Hsieh AL, et al. MYC, metabolism, and cancer. *Cancer Discov.* 2015;5:1024–39. <https://doi.org/10.1158/2159-8290.CD-15-0507>.
61. Dang CV. The interplay between MYC and HIF in the Warburg effect. *Ernst Schering Found Symp Proc.* 2007. https://doi.org/10.1007/2789_2008_088.
62. Mossmann D, Park S, Hall MN. mTOR signalling and cellular metabolism are mutual determinants in cancer. *Nat Rev Cancer.* 2018;18:744–57. <https://doi.org/10.1038/s41568-018-0074-8>.
63. Saxton RA, Sabatini DM. mTOR signaling in growth, metabolism, and disease. *Cell.* 2017;168:960–76. <https://doi.org/10.1016/j.cell.2017.02.004>.
64. Moritz A, Li Y, Guo A, Villen J, et al. Akt-RSK-S6 kinase signaling networks activated by oncogenic receptor tyrosine kinases. *Sci Signal.* 2010. <https://doi.org/10.1126/scisignal.2000998>.
65. Garcia-Maceira P, Mateo J. Silibinin inhibits hypoxia-inducible factor-1alpha and mTOR/p70S6K/4E-BP1 signaling pathway in human cervical and hepatoma cancer cells: implications for anticancer therapy. *Oncogene.* 2009;28:313–24. <https://doi.org/10.1038/onc.2008.398>.
66. Dodd KM, Yang J, Shen MH, Sampson JR, et al. mTORC1 drives HIF-1alpha and VEGF-A signalling via multiple mechanisms involving 4E-BP1, S6K1 and STAT3. *Oncogene.* 2015;34:2239–50. <https://doi.org/10.1038/onc.2014.164>.
67. Land SC, Tee AR. Hypoxia-inducible factor 1alpha is regulated by the mammalian target of rapamycin (mTOR) via an mTOR signaling motif. *J Biol Chem.* 2007;282:20534–43. <https://doi.org/10.1074/jbc.M611782200>.
68. Sun Q, Chen X, Ma J, Peng H, et al. Mammalian target of rapamycin up-regulation of pyruvate kinase isoenzyme type M2 is critical for aerobic glycolysis and tumor growth. *Proc Natl Acad Sci U S A.* 2011;108:4129–34. <https://doi.org/10.1073/pnas.1014769108>.
69. Chung SI, Moon H, Ju HL, Cho KJ, et al. Hepatic expression of Sonic Hedgehog induces liver fibrosis and promotes hepatocarcinogenesis in a transgenic mouse model. *J Hepatol.* 2016;64:618–27. <https://doi.org/10.1016/j.jhep.2015.10.007>.
70. Wang S, Wang Y, Xun X, Zhang C, et al. Hedgehog signaling promotes sorafenib resistance in hepatocellular carcinoma patient-derived organoids. *J Exp Clin Cancer Res.* 2020;39:22. <https://doi.org/10.1186/s13046-020-1523-2>.
71. Ding J, Li HY, Zhang L, Zhou Y, et al. Hedgehog signaling, a critical pathway governing the development and progression of hepatocellular carcinoma. *Cells.* 2021. <https://doi.org/10.3390/cells10010123>.
72. Wei X, Zhao L, Ren R, Ji F, et al. MiR-125b loss activated HIF1alpha/pAKT loop, leading to transarterial chemoembolization resistance in hepatocellular carcinoma. *Hepatology.* 2021;73:1381–98. <https://doi.org/10.1002/hep.31448>.
73. Martin SP, Fako V, Dang H, Dominguez DA, et al. PKM2 inhibition may reverse therapeutic resistance to transarterial chemoembolization in hepatocellular carcinoma. *J Exp Clin Cancer Res.* 2020;39:99. <https://doi.org/10.1186/s13046-020-01605-y>.
74. Highfill SL, Cui Y, Giles AJ, Smith JP, et al. Disruption of CXCR2-mediated MDSC tumor trafficking enhances anti-PD1 efficacy. *Sci Transl Med.* 2014. <https://doi.org/10.1126/scitranslmed.3007974>.
75. Chiu DK, Tse AP, Xu IM, Di Cui J, et al. Hypoxia inducible factor HIF-1 promotes myeloid-derived suppressor cells accumulation through ENTPD2/CD39L1 in hepatocellular carcinoma. *Nat Commun.* 2017;8:517. <https://doi.org/10.1038/s41467-017-00530-7>.
76. Lu C, Rong D, Zhang B, Zheng W, et al. Current perspectives on the immunosuppressive tumor microenvironment in hepatocellular carcinoma: challenges and opportunities. *Mol Cancer.* 2019;18:130. <https://doi.org/10.1186/s12943-019-1047-6>.
77. Yu SJ, Ma C, Heinrich B, Brown ZJ, et al. Targeting the crosstalk between cytokine-induced killer cells and myeloid-derived suppressor cells in hepatocellular carcinoma. *J Hepatol.* 2019;70:449–57. <https://doi.org/10.1016/j.jhep.2018.10.040>.
78. Hoechst B, Voigtlaender T, Ormandy L, Gamrekelashvili J, et al. Myeloid derived suppressor cells inhibit natural killer cells in patients with hepatocellular carcinoma via the NKp30 receptor. *Hepatology.* 2009;50:799–807. <https://doi.org/10.1002/hep.23054>.
79. Kalathil S, Lugade AA, Miller A, Iyer R, et al. Higher frequencies of GARP (+)CTLA-4 (+)Foxp3 (+)T regulatory cells and myeloid-derived suppressor cells in hepatocellular carcinoma patients are associated with impaired T-cell functionality. *Cancer Res.* 2013;73:2435–44. <https://doi.org/10.1158/0008-5472.CAN-12-3381>.
80. Chiu DK, Xu IM, Lai RK, Tse AP, et al. Hypoxia induces myeloid-derived suppressor cell recruitment to hepatocellular carcinoma through chemokine (C-C motif) ligand 26. *Hepatology.* 2016;64:797–813. <https://doi.org/10.1002/hep.28655>.

81. Jiang M, Chen J, Zhang W, Zhang R, et al. Interleukin-6 trans-signaling pathway promotes immunosuppressive myeloid-derived suppressor cells via suppression of suppressor of cytokine signaling 3 in breast cancer. *Front Immunol*. 2017;8:1840. <https://doi.org/10.3389/fimmu.2017.01840>.
82. Lu LC, Chang CJ, Hsu CH. Targeting myeloid-derived suppressor cells in the treatment of hepatocellular carcinoma: current state and future perspectives. *J Hepatocell Carcinoma*. 2019;6:71–84. <https://doi.org/10.2147/JHC.S159693>.
83. Xia S, Wu J, Zhou W, Zhang M, et al. SLC7A2 deficiency promotes hepatocellular carcinoma progression by enhancing recruitment of myeloid-derived suppressors cells. *Cell Death Dis*. 2021;12:570. <https://doi.org/10.1038/s41419-021-03853-y>.
84. Lin Y, Yang X, Liu W, Li B, et al. Chemerin has a protective role in hepatocellular carcinoma by inhibiting the expression of IL-6 and GM-CSF and MDSC accumulation. *Oncogene*. 2017;36:3599–608. <https://doi.org/10.1038/ncr.2016.516>.
85. Zhou J, Liu M, Sun H, Feng Y, et al. Hepatoma-intrinsic CCRK inhibition diminishes myeloid-derived suppressor cell immunosuppression and enhances immune-checkpoint blockade efficacy. *Gut*. 2018;67:931–44. <https://doi.org/10.1136/gutjnl-2017-314032>.
86. Deng Y, Cheng J, Fu B, Liu W, et al. Hepatic carcinoma-associated fibroblasts enhance immune suppression by facilitating the generation of myeloid-derived suppressor cells. *Oncogene*. 2017;36:1090–101. <https://doi.org/10.1038/onc.2016.273>.
87. Hsieh CC, Hung CH, Chiang M, Tsai YC, et al. Hepatic stellate cells enhance liver cancer progression by inducing myeloid-derived suppressor cells through interleukin-6 signaling. *Int J Mol Sci*. 2019. <https://doi.org/10.3390/ijms20205079>.
88. Barsoum IB, Smallwood CA, Siemens DR, Graham CH. A mechanism of hypoxia-mediated escape from adaptive immunity in cancer cells. *Cancer Res*. 2014;74:665–74. <https://doi.org/10.1158/0008-5472.CAN-13-0992>.

Publisher's Note

Springer Nature remains neutral with regard to jurisdictional claims in published maps and institutional affiliations.

Submit your manuscript to a SpringerOpen[®] journal and benefit from:

- ▶ Convenient online submission
- ▶ Rigorous peer review
- ▶ Open access: articles freely available online
- ▶ High visibility within the field
- ▶ Retaining the copyright to your article

Submit your next manuscript at ▶ [springeropen.com](https://www.springeropen.com)
